Acta Crystallographica Section D
Biological Crystallography
ISSN 0907-4449

Structural polymorphism of c-di-GMP bound to an EAL domain and in complex with a type II PilZ-domain protein

Ko-Hsin Chin,[a] Wei-Ting Kuo,[b] Yu-Jen Yu,[b] Yi-Ting Liao,[b] Ming-Te Yang[c] and Shan-Ho Chou[a,b,d]*

[a]Agricultural Biotechnology Center, National Chung Hsing University, Taichung 40227, Taiwan, [b]Institute of Biochemistry, National Chung Hsing University, Taichung 40227, Taiwan, [c]Institute of Molecular Biology, National Chung Hsing University, Taichung 40227, Taiwan, and [d]Graduate Institute of Basic Medical Science, China Medical University, Taichung 40402, Taiwan

Correspondence e-mail: shchou@nchu.edu.tw

Received 15 May 2012
Accepted 4 July 2012

PDB References: *Xcc*Fim-FimX^{EAL}–c-di-GMP, 4f3h; *Xcc*FimX^{EAL}–c-di-GMP–XccPilZ, 4f48

Cyclic di-GMP (c-di-GMP) is a novel secondary-messenger molecule that is involved in regulating a plethora of important bacterial activities through binding to an unprecedented array of effectors. Proteins with a canonical PilZ domain that bind c-di-GMP play crucial roles in regulating flagellum-based motility. In contrast, noncanonical type II PilZ domains that do not effectively bind c-di-GMP regulate twitching motility, which is dependent on type IV pili (T4P). Recent data indicate that T4P biogenesis is initiated *via* the interaction of a non-canonical type II PilZ protein with the GGDEF/EAL-domain protein FimX and the pilus motor protein PilB at high c-di-GMP concentrations. However, the molecular details of such interactions remain to be elucidated. In this manuscript, the first hetero-complex crystal structure between a type II PilZ protein and the EAL domain of the FimX protein (FimX^{EAL}) from *Xanthomonas campestris* pv. *campestris* (*Xcc*) in the presence of c-di-GMP is reported. This work reveals two novel conformations of monomeric c-di-GMP in the *Xcc*FimX^{EAL}–c-di-GMP and *Xcc*FimX^{EAL}–c-di-GMP–*Xcc*PilZ complexes, as well as a unique interaction mode of a type II PilZ domain with FimX^{EAL}. These findings indicate that c-di-GMP is sufficiently flexible to adjust its conformation to match the corresponding recognition motifs of different cognate effectors. Together, these results represent a first step towards an understanding of how T4P biogenesis is controlled by c-di-GMP at the molecular level and also of the ability of c-di-GMP to bind to a wide variety of effectors.

1. Introduction

Cyclic di-GMP is a unique secondary messenger that controls many important cellular activities in diverse bacteria (Römling *et al.*, 2005; Jenal & Malone, 2006; Römling & Amikam, 2006; Hengge, 2009; Schirmer & Jenal, 2009). However, the mechanisms by which c-di-GMP exerts its regulatory effect are incompletely understood. A wide variety of different protein-based or RNA-based recognition motifs for c-di-GMP have been discovered. Some representative examples include the transcription factors Clp (Chin *et al.*, 2010), RNA-processing polynucleotide phosphorylase (PNPase; Tuckerman *et al.*, 2011), degenerate GGDEF- or EAL-domain proteins (where degenerate means that they contain a modified GGDEF or EAL motif in the active site and become inactive as enzymes, but still exhibit sufficient

binding affinity to c-di-GMP to serve as an effector; Navarro *et al.*, 2011), PilZ-domain proteins (Benach *et al.*, 2007; Li, Chin, Liu *et al.*, 2009) and riboswitches (Smith *et al.*, 2011). The search for novel c-di-GMP receptors is still ongoing (Römling, 2011; Sondermann *et al.*, 2011; Ryan *et al.*, 2012).

C-di-GMP regulates motility, which is an important trait for bacterial survival and pathogenicity (Thormann & Paulick, 2010). Recently, a number of studies have described the molecular basis of c-di-GMP-induced alteration of swimming motility, which depends upon flagella. It is found that c-di-GMP binds to the type I PilZ-domain protein YcgR, which then interacts with the flagellar machinery proteins to set a 'brake' on smooth bacterial motion (Boehm *et al.*, 2010; Fang & Gomelsky, 2010; Paul *et al.*, 2010). In contrast, although bacterial twitching motility also requires PilZ-domain proteins (Alm *et al.*, 1996; Mattick, 2002), these are classified as type II as they lack the canonical sequences required for c-di-GMP binding and are unable to interact directly with c-di-GMP (Guzzo *et al.*, 2009; Li, Chin, Liu *et al.*, 2009). In *Xanthomonas campestris* pv. *campestris* (*Xcc*), four PilZ proteins were found to be essential for pathogenicity (McCarthy *et al.*, 2008). Two of these PilZ proteins contain a canonical type I PilZ domain, while the other two contain a type II noncanonical PilZ domain. *Xcc*PilZ$_{1028}$ is a type II PilZ domain that is monomeric in nature (Li, Chin, Liu *et al.*, 2009), while *Xcc*PilZ$_{6012}$ is a type II PilZ domain that is tetrameric (Li *et al.*, 2011).

FimX is another protein that is essential for governing bacterial twitching motility (Huang *et al.*, 2003; Kazmierczak *et al.*, 2006) and has been identified as a high-affinity c-di-GMP-binding receptor (Navarro *et al.*, 2009; Qi *et al.*, 2011). It contains a degenerate GGDEF domain, as well as a degenerate EAL domain, which is implicated in binding c-di-GMP. Crystal structures of *Pa*FimX^{EAL} and a *Pa*FimX^{EAL}–c-di-GMP complex have recently been reported (Navarro *et al.*, 2009). Importantly, work on *X. xonopodis* pv. *citri* (*Xac*) has suggested that the type II *Xac*PilZ serves as a mediator to connect the pilus motor protein ATPase *Xac*PilB to the EAL domain of an *Xac* homologue of FimX (Guzzo *et al.*, 2009). The molecular details of how the binding of c-di-GMP to the FimX protein influences the PilZ domain and leads to control of T4P biogenesis is unclear.

The *Xac*PilZ sequence is identical to that of *Xcc*PilZ$_{1028}$ (Guzzo *et al.*, 2009; Li, Chin, Liu *et al.*, 2009), and *Xac*FimX^{EAL} also has high sequence similarity to *Xcc*FimX^{EAL}, suggesting that comparable interactions between the FimX^{EAL} and PilZ domains are likely to occur in *Xcc*. In the current manuscript, we report the structural characterization of the *Xcc*FimX^{EAL}–c-di-GMP and *Xcc*PilZ$_{1028}$–*Xcc*FimX^{EAL}–c-di-GMP complexes in order to explore this intriguing issue. The results show that c-di-GMP is indispensable for the stable formation of the type II *Xcc*PilZ$_{1028}$–*Xcc*FimX^{EAL} complex, which forms a (*Xcc*PilZ$_{1028}$)$_2$–(*Xcc*FimX^{EAL}–c-di-GMP)$_2$ heterotetramer *via* domain swapping of the *Xcc*FimX^{EAL} N-terminal α-helix. Two novel monomeric c-di-GMP conformations were discovered in this study, demonstrating the conformational flexibility of c-di-GMP as an additional parameter in accomplishing its diverse functions.

2. Materials and methods

2.1. The cloning, expression and purification of native and SeMet-labelled *Xcc*FimX^{EAL} and *Xcc*PilZ$_{1028}$

The cloning, expression, purification, crystallization and data collection of native and SeMet-labelled *Xcc*FimX^{EAL} and *Xcc*PilZ$_{1028}$ have been described in previous publications (Li, Chin, Shih *et al.*, 2009; Liao *et al.*, 2012). In brief, *Xcc*FimX^{EAL} was directly PCR-amplified from the plant pathogen *X. campestris* pv. *campestris* strain 17. A ligation-independent cloning (LIC) approach (Wu *et al.*, 2005) was used to obtain the desired constructs. A series of substitutions of amino-acid residues in the *Xcc*FimX^{EAL} and *Xcc*PilZ$_{1028}$ proteins were carried out using the QuikChange site-directed mutagenesis method (Stratagene) with *Pfu* Ultra DNA polymerase (Stratagene). The forward and reverse oligonucleotide primers used in the mutagenesis experiments are listed in Supplementary Table S1.[1] Appropriate mutations were confirmed by DNA sequencing.

2.2. Reagents

C-di-GMP was produced by an enzymatic method using an altered thermophilic DGC enzyme as described previously (Rao *et al.*, 2009).

2.3. X-ray data collection

The single anomalous dispersion (SAD) method was used to determine the structure of the SeMet-*Xcc*FimX^{EAL}–c-di-GMP–*Xcc*PilZ complex. The data were indexed and integrated using the *HKL*-2000 processing software (Otwinowski & Minor, 1997), generating data sets that were approximately 99.4% complete. The refinement of Se-atom positions, phase calculation and density modification were carried out using the programs *SHARP* and *autoSHARP* (de La Fortelle & Bricogne, 1997) The model was manually adjusted using the *XtalView*/*Xfit* package (McRee, 1999). *REFMAC*5 (Murshudov *et al.*, 2011) was then used for refinement to a final R_{cryst} of 23.8% and R_{free} of 27.2%. The determined *Xcc*FimX^{EAL} structure was then used as a model to determine the structure of the *Xcc*FimX^{EAL}–c-di-GMP–*Xcc*PilZ$_{1028}$ complex using a molecular-replacement approach (Adams *et al.*, 2010). The obtained complex model was refined in a similar iterative way. The data-collection and refinement statistics are summarized in Table 1.

2.4. ITC measurements of wild-type *Xcc*FimX^{EAL} and *Xcc*PilZ$_{1028}$ and their variants

A sample of *Xcc*FimX^{EAL} for ITC was extensively dialyzed against assay buffer (40 m*M* NaCl, 10 m*M* Tris pH 8.0, 0.5 m*M* $MgCl_2$) to prevent contamination with c-di-GMP (Qi *et al.*, 2011). The protein samples were first diluted with the assay buffer to 30 μ*M* before loading into the ITC cell. C-di-GMP was diluted in the same way to 0.5 m*M* before loading into the

[1] Supplementary material has been deposited in the IUCr electronic archive (Reference: EN5501). Services for accessing this material are described at the back of the journal.

Table 1
Data-collection and structure-refinement statistics for the *Xcc*FimX^{EAL}–c-di-GMP and SeMet-*Xcc*FimX^{EAL}–c-di-GMP–*Xcc*PilZ$_{1028}$ complexes.

Values in parentheses are for the outermost shell.

	*Xcc*FimX^{EAL}–c-di-GMP	SeMet-*Xcc*FimX^{EAL}–c-di-GMP–*Xcc*PilZ$_{1028}$
	Native†	Peak
Beamline	BL13B1, NSRRC	BL12B, SPring-8
Wavelength (Å)	1.00000	0.97934
Space group	$P3_221$	$P6_322$
Unit-cell parameters (Å)	$a = b = 65.665$, $c = 121.289$	$a = b = 158.222$, $c = 64.807$
Resolution range (Å)	30–2.5 (2.59–2.50)	30–2.7 (2.80–2.70)
Unique observations	68379 (10869)	189837 (49419)
Multiplicity	6.3 (5.5)	3.8 (3.3)
Completeness (%)	98.7 (98.2)	99.4 (98.7)
R_{merge}‡ (%)	3.6 (22.1)	13.8 (55.2)
$\langle I/\sigma(I)\rangle$	38.8 (7.1)	7.8 (1.8)
Refinement statistics		
R_{cryst}/R_{free}§ (%)	22.8/26.5	23.8/27.2
Model content		
Protein residues	241	340
Waters	116	243
c-di-GMP	1	1
B factors (Å^2)		
Backbone atoms	61.5	57.5
Side-chain atoms	77.4	68.9
Water O atoms	67.6	54.6
Ramachandran plot, residues in (%)		
Most favourable regions	90.5	91.5
Additionally allowed regions	9.1	7.6
Generously allowed regions	0.4	0.9
R.m.s.d. from ideal geometry		
Bonds (Å)	0.015	0.010
Angles (°)	1.45	1.38

† Friedel mates were considered separately as unique reflections in the calculation of these statistics. ‡ $R_{merge} = \sum_{hkl}\sum_i |I_i(hkl) - \langle I(hkl)\rangle|/\sum_{hkl}\sum_i I_i(hkl)$. § R_{free} is the same as R_{cryst} but for 5.0% of the total reflections that were chosen at random and omitted from refinement.

syringe. 2 µl c-di-GMP solution was then injected into the cell at 3 min intervals. ITC experiments on wild-type *Xcc*FimX^{EAL} and variants were all carried out at 298 K and the data were fitted using the commercial *Origin* 7.0 program to obtain ΔH and K_d values. Titrations of the *Xcc*FimX^{EAL}–c-di-GMP complex with *Xcc*PilZ$_{1028}$ were carried out in a similar way. The ITC measurement data for titrations of *Xcc*FimX^{EAL} and its variants with c-di-GMP and of the *Xcc*FimX^{EAL}–c-di-GMP complex with *Xcc*PilZ$_{1028}$ and its variants are listed in Tables 2 and 3, respectively.

3. Results

3.1. *Xcc*FimX^{EAL} is a degenerate c-di-GMP phosphodiesterase (PDE)

Sequence alignments between *Xcc*FimX^{EAL} and other active PDEs containing the EAL motif such as RocR, YkuI and tdEAL (data not shown) indicate that *Xcc*FimX^{EAL} is a potential degenerate PDE as it contains a highly modified QAF motif in the active site (highlighted in green in Fig. 1*a*). In addition, the three highly conserved residues involved in magnesium-ion coordination in active PDEs such as YkuI (residues Asn88, Asp122 and Asp152; Minasov *et al.*, 2009) or tdEAL (residues Asn584, Glu616 and Asp646; Tchigvintsev *et al.*, 2010) have been modified to Arg97, Gln129 and Glu159 in *Xcc*FimX^{EAL} (highlighted in cyan in Fig. 1*a*), respectively. Besides, no metal ion can be identified in the active-site region of the map. These findings, along with the observation that no enzymatic activity can be detected for *Xcc*FimX^{EAL} (data not shown), indicate that *Xcc*FimX^{EAL} is a degenerate PDE. Yet, similar to the FimX^{EAL} domain from *Pseudomonas aeruginosa* (Navarro *et al.*, 2009; Qi *et al.*, 2011), wild-type *Xcc*FimX^{EAL} can bind c-di-GMP very well, with a K_d in the micromolar range as determined using the ITC method (Table 2).

Table 2
ITC titration of the *Xcc*FimX^{EAL} variants with c-di-GMP.

FimX^{EAL} variant	Solubility and stability	Affinity measurable by ITC	Dissociation constant (K_d)
Wild type	OK	Yes	4.2×10^{-7}
Q40A	OK	No	NA
F42A	Degraded	NA	NA
S53A	OK	Yes	1.5×10^{-7}
R97A	OK	Yes	2.6×10^{-6}
E159A	Degraded	NA	NA
E216A	Insoluble	NA	NA
F217A	OK	No	NA

Table 3
ITC titration of the c-di-GMP–*Xcc*FimX^{EAL} complex with *Xcc*PilZ variants.

*Xcc*PilZ variant	Solubility and stability	Affinity measurable by ITC	Dissociation constant (K_d)
Wild type	OK	Yes	3.2×10^{-6}
G45A	OK	No	NA
G45V	Degraded	No	NA
K30A	OK	No	NA
K66A	OK	No	NA

3.2. The crystal structure of the *Xcc*FimX^{EAL}–c-di-GMP complex exhibits a novel bulged c-di-GMP conformation

*Xcc*FimX comprises REC, PAS, GGDEF and EAL domains. We have constructed a series of *Xcc*FimX variants containing different domain combinations and attempted to crystallize them in the absence or presence of c-di-GMP (Liao *et al.*, 2012). Unfortunately, most of these constructs did not produce suitable crystals for X-ray diffraction study. Only the *Xcc*FimX^{EAL} domain could be crystallized in the presence of c-di-GMP; these crystals diffracted to a resolution of 2.5 Å (Liao *et al.*, 2012).

The overall fold of the degenerate EAL domain containing a modified active-site QAF motif in the *Xcc*FimX^{EAL}–c-di-GMP complex is similar to the degenerate *Pa*FimX^{EAL} domain containing a modified EVL motif (PDB entry 3hv8; Navarro *et al.*, 2009) and the degenerate *Pf*LapD^{EAL} domain containing a modified KVL motif (PDB entry 3pjt) from *P. fluorescens* (Navarro *et al.*, 2011; Fig. 1*b*). Despite low sequence identity (26 and 31% with 3pjt and 3hv8, respec-

tively; Fig. 1*a*), *Xcc*FimX^{EAL} superimposes well with the *Pa*FimX^{EAL} and *Pf*LapD^{EAL} domains, with r.m.s.d.s of 1.55 Å over 183 C$^{\alpha}$ positions and 1.36 Å over 207 C$^{\alpha}$ positions, respectively. The *Xcc*FimX^{EAL} domain also contains eight β-strands and 11 α-helices, which interact efficiently to form a TIM-like barrel. Contrary to the classical $(\beta/\alpha)_8$ TIM-barrel fold (Sterner & Höcker, 2005) and similar to the degenerate *Pa*FimX^{EAL} and *Pf*LapDX^{EAL} domains, the *Xcc*FimX^{EAL} domain adopts a modified $\alpha\beta(\beta/\alpha)_6\beta$ barrel with the first β-strand running antiparallel to the other seven β-strands. In addition, the *Xcc*FimX^{EAL} domain lacks α-helices at the β1-strand face, which may facilitate interactions of such a modified TIM-like barrel with other cognate partners *via* this side. Furthermore, a small extra β-strand ($\beta2'$) is found located between the β2 strand and the α2 helix (Fig. 1*b*). This extra $\beta2'$ strand is found to be important in interacting with the *Xcc*PilZ$_{1028}$ protein to form the *Xcc*FimX^{EAL}–c-di-GMP–*Xcc*PilZ$_{1028}$ complex (see subsequent description). Important residues that are involved in binding with c-di-GMP are shown in stick representation in Fig. 1(*b*).

Since the *Xcc*FimX^{EAL} crystals could only be grown in the presence of c-di-GMP, and a substantial extra electron-density patch was detected at the C-terminal end of the β-strands comprising the barrel, we modelled a c-di-GMP molecule into the electron density at the active site. Indeed, c-di-GMP was found to fit very well into this electron-density patch after considerable conformational adjustment of the second guanine base (Gua2; Fig. 2*a*). The adjusted c-di-GMP conformation was found to adopt a novel 'bulged' conformation, which was obtained with high confidence since the model fits well to the electron-density map contoured at the 3σ level (Fig. 2*a*). When plotted as van der Waals spheres, the charged groups and hydrophobic groups of c-di-GMP were found to complement the the *Xcc*FimX^{EAL} active site drawn in electrostatic potential representation (Fig. 2*b*). Surprisingly, unlike the guanine bases that adopt a normal *anti* conformation in all monomeric and dimeric c-di-GMP structures reported to date, the Gua2 base in this novel conformation adopts an unusual *syn* conformation which is characterized by a short distance of 2.52 Å between the sugar anomeric C1′ and base C8 atoms (marked by blue dotted arrows in Fig. 2*b*).

Although unique, the bulged c-di-GMP is still able to interact extensively with the surrounding residues in the *Xcc*FimX^{EAL} active site, as shown in Fig. 2(*c*). Except for the conserved residues Asp71 and Arg44 of the FimX^{EAL} sequences (Fig. 1*a*), which interact with the Gua1 base and the upper phosphate moiety (Fig. 2), respectively, the residues

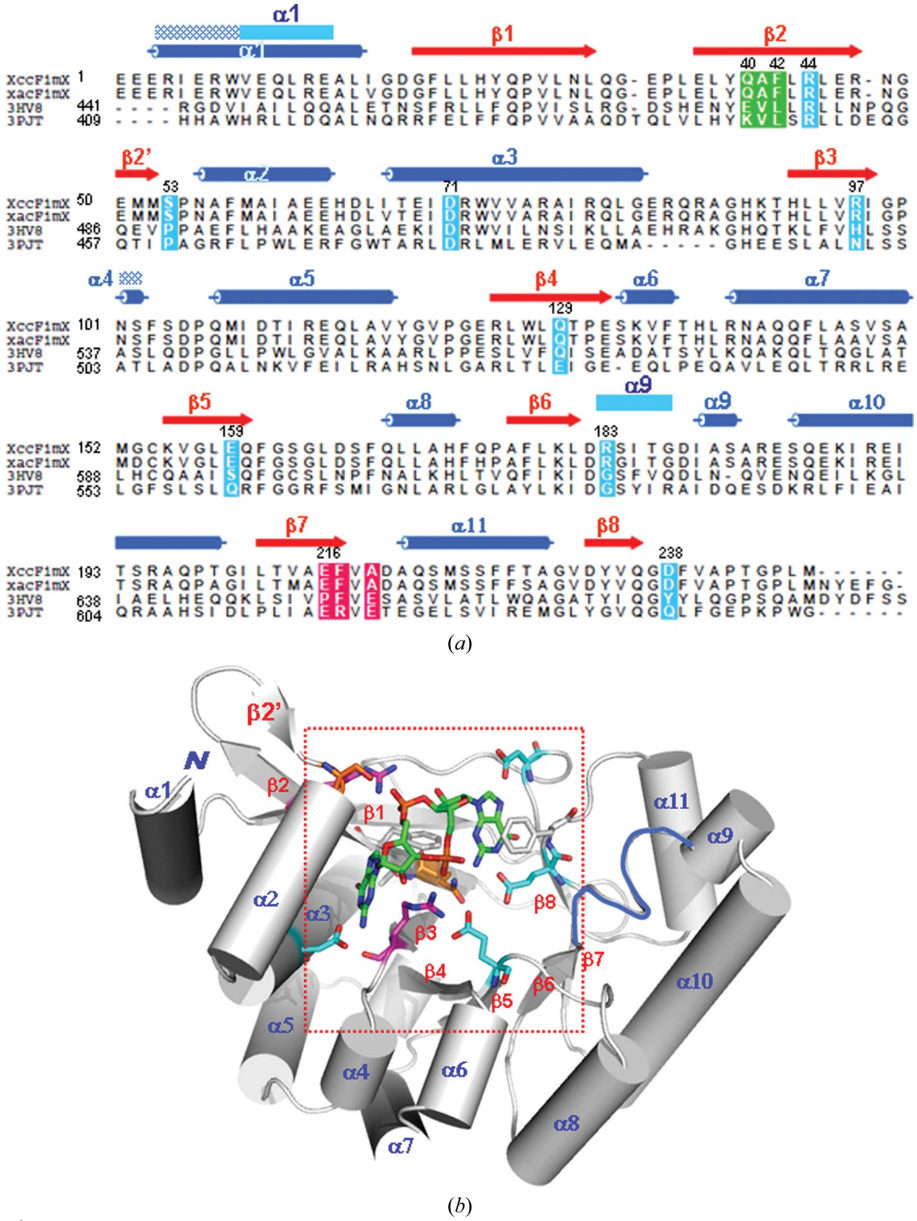

Figure 1
(*a*) Sequence alignments of degenerate EAL domains from *Xcc*, *Xac*, *P. aeruginosa* (PDB entry 3hv8) and *P. fluorescens* (PDB entry 3pjt) and locations of the secondary-structure elements in *Xcc*FimX^{EAL}. Residues important for interaction with the c-di-GMP molecule are highlighted in green for the EAL motifs, in blue for residues forming hydrogen bonds or electrostatic bonds and in magenta for the tetraresidue motif that is possibly involved in conferring the unique bulged or open-*syn* conformation of c-di-GMP. (*b*) Crystal structure of the *Xcc*FimX^{EAL}–c-di-GMP complex with the backbone drawn in grey cartoon except for the $\beta6$–$\alpha9$ loop region, which is coloured blue. This region becomes the $\alpha9$ helix after binding to *Xcc*PilZ$_{1028}$. Residues in the *Xcc*FimX^{EAL} domain important in interaction with the c-di-GMP molecule are drawn in stick representation. C atoms of positively charged residues are shown in magenta, of negatively charged residues in cyan, of polar residues in orange, of hydrophobic residues in grey and those in c-di-GMP in green.

that coordinate to the metal ion in active PDEs have been modified to Gln129 and Glu159, which now form a hydrogen-bonding network to position another modified residue Arg97 in an optimum position to bind to the lower phosphate moiety of c-di-GMP. In particular, Gua2 of the bulged c-di-GMP was found to interact with the degenerate *Xcc*FimX^{EAL} domain in a unique way (see also Supplementary Table S2 and Fig. S4). It is well stacked by the phenyl ring of Phe217 and is hydrogen-bonded extensively using its base-edge heteroatoms to the side-chain carboxylates of Glu216 and Asp238 and the main-chain atom of Phe217. This unique c-di-GMP conformer is thus well accommodated in the active site, accompanied by many interactions from residues Arg44 in the $\beta2$ strand, Ser53 in the $\beta2'$ strand, Asp71 in the $\alpha3$ helix, Arg97 in the $\beta3$ strand, Glu216 in the $\beta7$ strand and Asp238 in the $\beta8$ strand (Fig. 2*c*). Such abundant interactions can account for the strong binding affinity (K_d = 0.42 μM) between the degenerate *Xcc*FimX^{EAL} domain and c-di-GMP. The determined crystal complex structure is also consistent with the ITC results measured on a series of *Xcc*FimX^{EAL} variants (Table 2). Most of the variants with replacements of crucial amino-acids in the ligand-binding site have reduced binding affinities, undergo protein degradation or become insoluble, indicating that the correct folding of the active site is important for *Xcc*FimX^{EAL} stability.

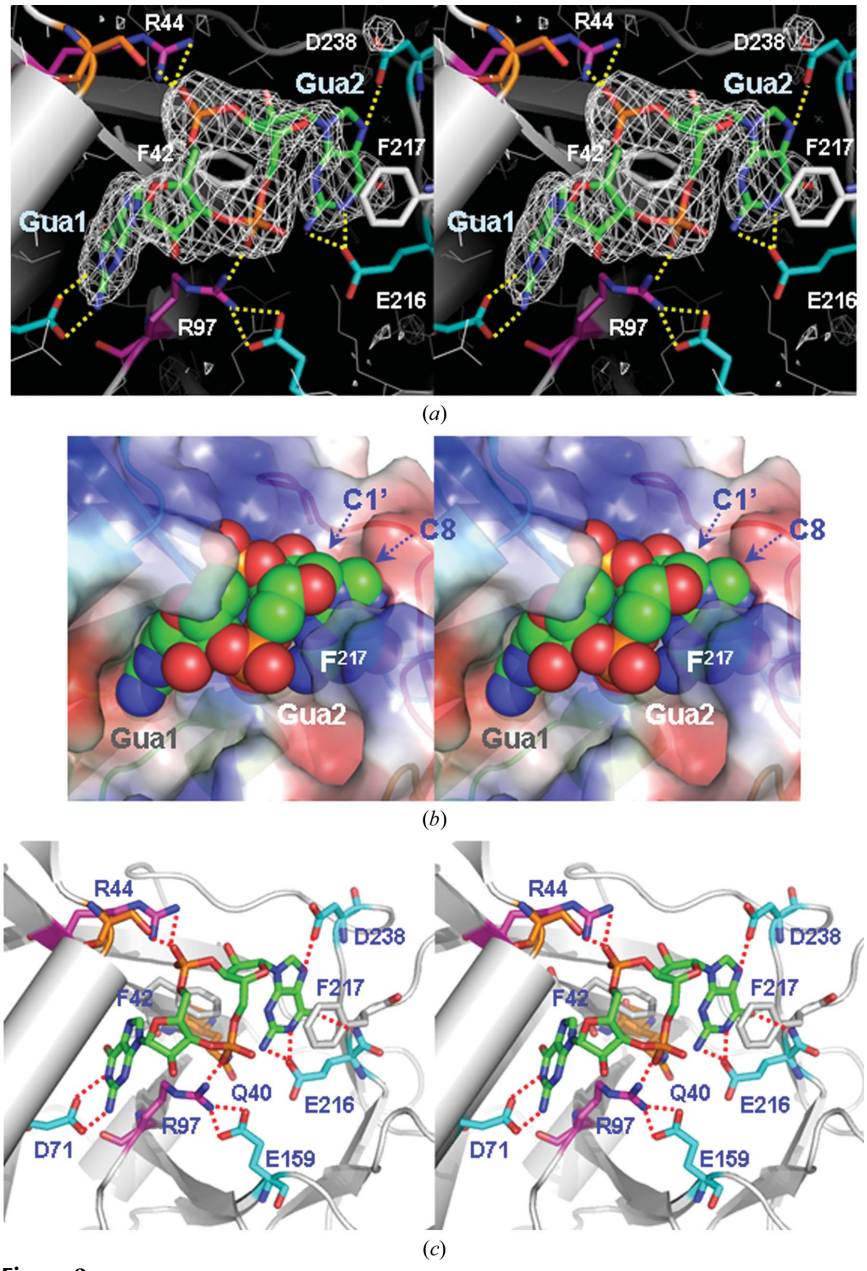

Figure 2
(*a*) Stereoview of the $F_o - F_c$ OMIT map of c-di-GMP contoured at 3σ. The molecular structure of c-di-GMP is embedded in the map. The colour code is similar to that in Fig. 1. The phenyl rings of Phe217 and Phe42 stack very well with the Gua2 base and the 12-membered ring of c-di-GMP, respectively. (*b*) Stereoview of the c-di-GMP molecule drawn as van der Waals spheres (negatively charged atoms in red, positively charged atoms in blue and C atoms in green) and fitted into the *Xcc*FimX^{EAL} active site drawn in electrostatic potential representation. The unique open-*syn* conformation of the c-di-GMP is clearly demonstrated by the close contact of the ribose C1′ and base C8 atoms (distance of 2.52 Å), which are marked by blue dotted arrows. (*c*) An expanded stereoview of the *Xcc*FimX^{EAL} active-site residues interacting with c-di-GMP. The colour code used is similar to that in Fig. 1(*b*). Hydrogen bonds and electrostatic bonds are connected by dotted lines in red.

The *Xcc*FimX^{EAL} domain is inactive with respect to PDE activity since it contains a unique QAF motif at the active site (Fig. 1*a*). However, this modified QAF motif does not seem to affect c-di-GMP binding greatly, as *Xcc*FimX^{EAL} still binds c-di-GMP well with a K_d in the low micromolar range, similar to those of the degenerate *Pa*FimX^{EAL}–c-di-GMP or *Pf*LapD^{EAL}–c-di-GMP complexes containing the modified EVL or KVL motifs (Navarro *et al.*, 2009, 2011). The distances of the side-chain atoms of the first Gln and second Ala residues to c-di-GMP are larger than 5 Å. Only the aromatic ring of the Phe42 residue in the QAF motif seems to serve as an excellent platform to accommodate the 12-membered ring of c-di-GMP (Figs. 2*a* and 2*c*). This effect is similar to that exhibited by the third-position Leu residue in the canonical EAL domain. However, the first Gln residue does seem to play an important role in binding c-di-GMP, as the *Xcc*FimX^{EAL} Q40A variant almost lost its ability to bind c-di-GMP (Table 2). The reason for the importance of the Gln residue in the QAF motif is unclear at present.

Detailed interactions between *Xcc*FimX^{EAL} and c-di-GMP are shown in Supplementary Table S2 and Fig. S4. It is clear from this study that c-di-GMP is flexible enough to adopt different conformations when bound to effector proteins that have similar functions but subtle sequence

differences. The discovery of this novel bulge-like and open-*syn* conformation of c-di-GMP (Fig. 6) is consistent with the view that the c-di-GMP conformation is sufficiently flexible (Zhang *et al.*, 2006; Wang *et al.*, 2010) to add another level of complexity to its interaction with many different effectors (Römling, 2011).

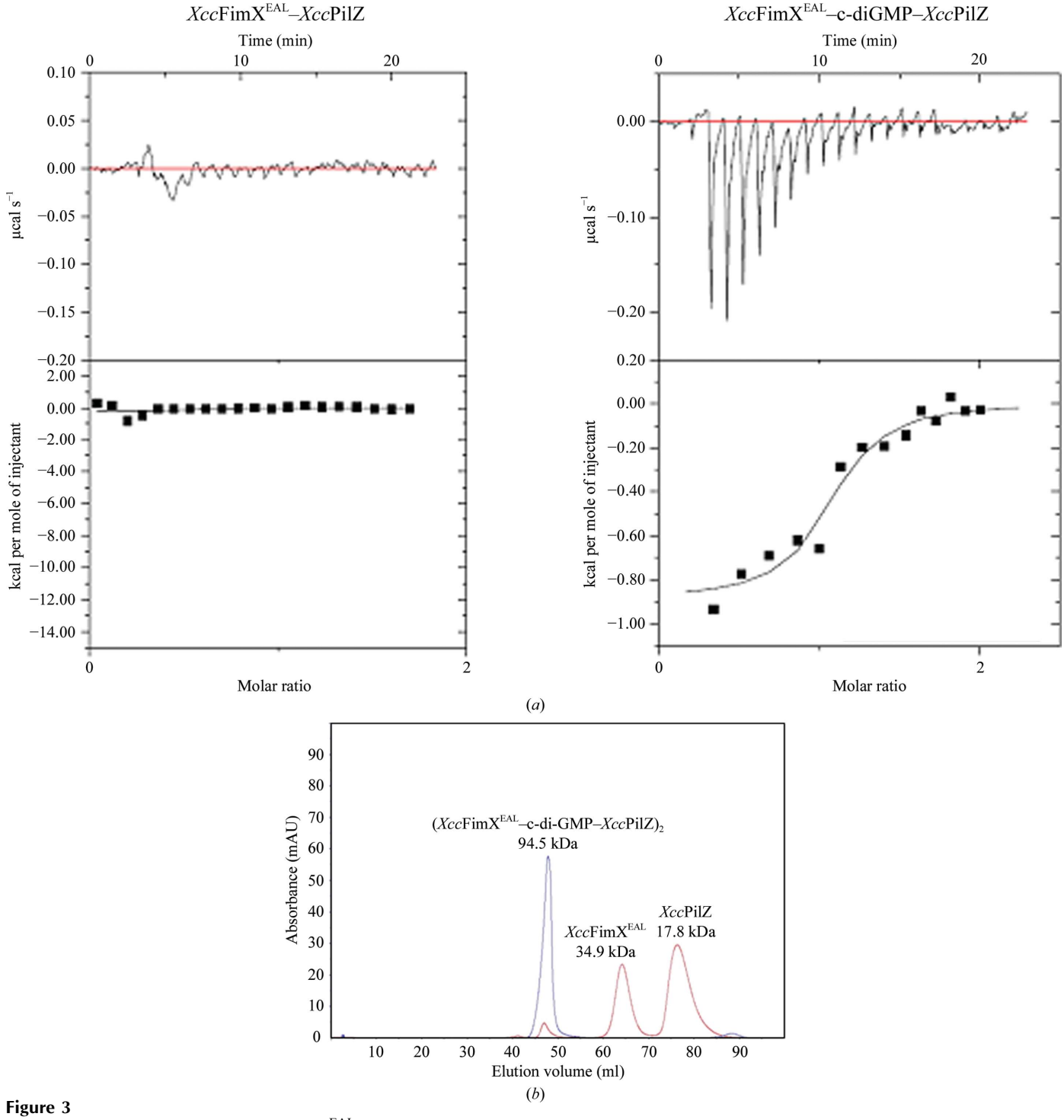

Figure 3
ITC and gel-filtration studies of the *Xcc*FimX^{EAL}–c-di-GMP–*Xcc*PilZ$_{1028}$ complex. (*a*) The heat released during the titration and the fitted curves for *Xcc*FimX^{EAL}–*Xcc*PilZ$_{1028}$ complex formation in the absence (left) and the presence (right) of c-di-GMP. No apparent heat was released when *Xcc*PilZ$_{1028}$ was titrated into reservoir solution containing the *Xcc*FimX^{EAL} domain only. However, significant heat release was observed when *Xcc*PilZ$_{1028}$ was titrated into *Xcc*FimX^{EAL}–c-di-GMP solution in an approximately 1:1 ratio. 1 cal = 4.186 J. (*b*) Gel-filtration elution profile of the *Xcc*FimX^{EAL} and *Xcc*PilZ$_{1028}$ proteins in the absence (red) and presence (blue) of c-di-GMP using a Superdex 75 column. The calibrated molecular weights of individual proteins and their complexes are marked at the top of the peak. In the absence of c-di-GMP only a minute amount of complex was present. In the presence of a proportional amount of c-di-GMP, however, only a single peak with a molecular weight approximately twice that of the *Xcc*FimX^{EAL}–c-di-GMP–*Xcc*PilZ$_{1028}$ complex was observed.

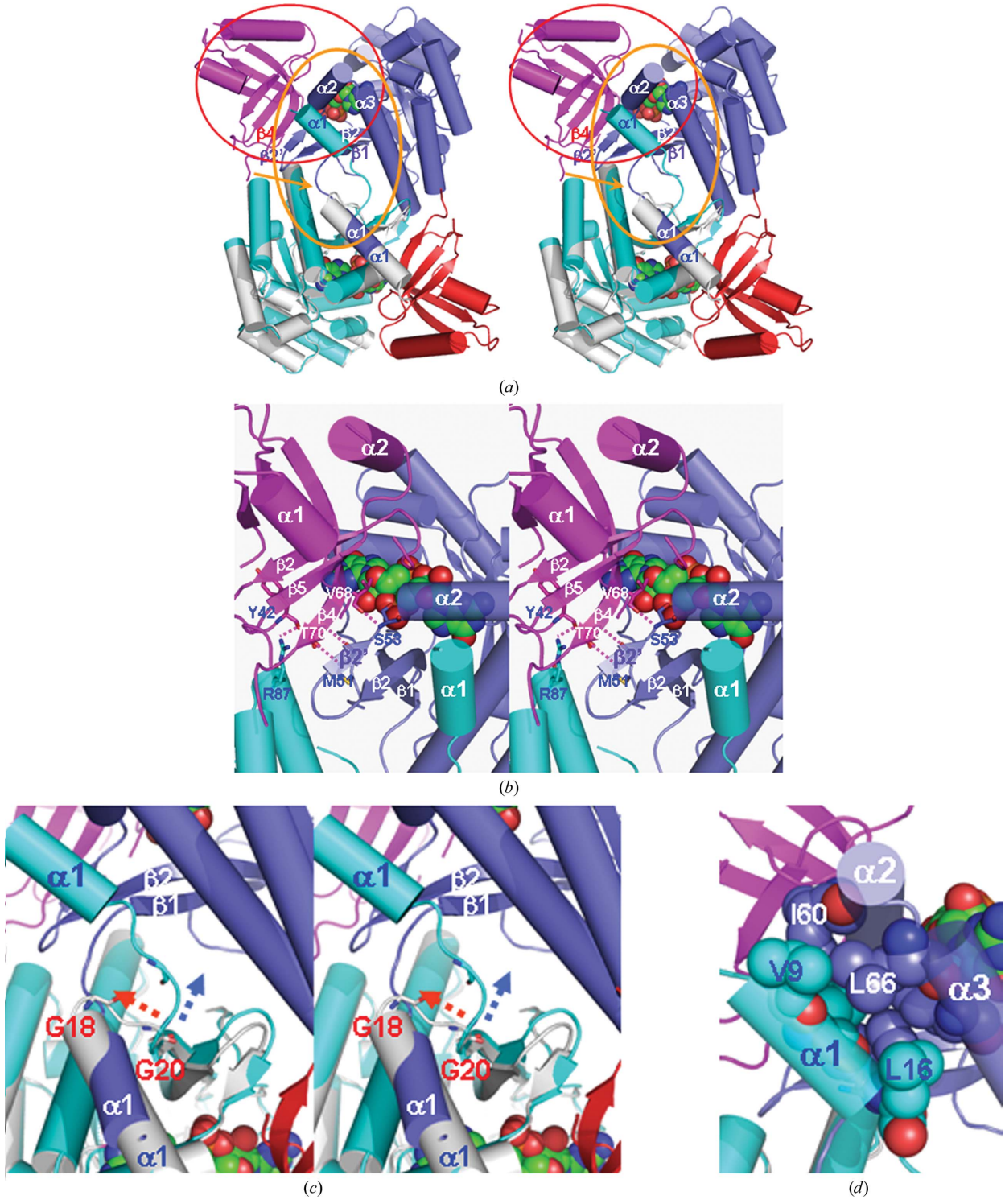

Figure 4
(*a*) Stereoview of the *Xcc*FimX^{EAL}–c-di-GMP–*Xcc*PilZ$_{1028}$ complex dimer. c-di-GMPs are drawn as van der Waals spheres and the *Xcc*FimX^{EAL} and *Xcc*PilZ$_{1028}$ domains are drawn in cartoon representation in cyan or marine and red or magenta, respectively. One *Xcc*FimX^{EAL}–c-di-GMP complex structure is also superimposed and drawn in grey in the lower left corner. The pseudo-β-sheet formed between the *Xcc*FimX^{EAL} and *Xcc*PilZ$_{1028}$ β-strands is circled in magenta and the domain swapping of the N-terminal α-helices of the *Xcc*FimX^{EAL} domains is circled in orange. (*b*) Expanded view of the pseudo-β-sheet formed between the *Xcc*FimX^{EAL} $\beta1$–$\beta2$–$\beta2'$ strands and the *Xcc*PilZ$_{1028}$ $\beta2$–$\beta5$–$\beta4$ strands. Hydrogen-bonding interactions are connected by dotted lines in magenta. (*c*) Expanded superimposed view of the *Xcc*FimX^{EAL} domain before $\alpha1$-helix swapping (grey cartoon) and after $\alpha1$-helix swapping (marine cartoon). Before *Xcc*PilZ$_{1028}$ binding, the $\alpha1$ helix turns leftwards after the hinge residue Gly20 (indicated by a dotted arrow in red) and continues to residue Gly18, making a sharp turn to interact with its own $\alpha2$ and $\alpha3$ helices. After *Xcc*PilZ$_{1028}$ binding, the $\alpha1$ helix swaps its direction after the hinge residue Gly20 (it instead turns rightwards as indicated by the blue dotted arrow) to interact with the $\alpha2$ and $\alpha3$ helices of the adjacent *Xcc*FimX^{EAL} domain. (*d*) Strong hydrophobic interactions between the swapped $\alpha1$ helix and the $\alpha2$ and $\alpha3$ helices of the adjacent *Xcc*FimX^{EAL} domain.

3.3. The *Xcc*PilZ$_{1028}$ domain does not bind c-di-GMP or isolated *Xcc*FimX^{EAL} but binds strongly to the *Xcc*FimX^{EAL}–c-di-GMP complex

Since c-di-GMP has been found to be important for bacterial twitching motility and since knockout of either noncanonical type II PilZ (Alm *et al.*, 1996; McCarthy *et al.*, 2008; Guzzo *et al.*, 2009) or FimX domains (Huang *et al.*, 2003; Kazmierczak *et al.*, 2006; Guzzo *et al.*, 2009) leads to dysfunction of T4P biogenesis, it is of interest to determine whether a type II PilZ domain can bind to isolated FimX^{EAL}, c-di-GMP or the FimX^{EAL}–c-di-GMP complex. *Xcc*PilZ$_{1028}$ is a type II PilZ domain that lacks the characteristic c-di-GMP binding signature motifs and accordingly exhibits no direct c-di-GMP binding, as confirmed by a previous ITC measurement (Li, Chin, Liu *et al.*, 2009). *Xcc*PilZ$_{1028}$ also exhibits only weak binding to the purified *Xcc*FimX^{EAL} domain, but interacts strongly with the *Xcc*FimX^{EAL} domain when c-di-GMP is present. This is clearly verified from the results of ITC and gel-filtration chromatography (Superdex 75; Fig. 3). Fig. 3(*a*) shows ITC data for the interaction of type II *Xcc*PilZ$_{1028}$ and *Xcc*FimX^{EAL} in the absence (left panel) and the presence (right panel) of c-di-GMP. Clearly, when c-di-GMP is absent no binding could be detected by the ITC method. However, a good binding affinity (K_d = 3.2 μ*M*) is observed when c-di-GMP is present in a 1:1 ratio with the *Xcc*PilZ$_{1028}$ and *Xcc*FimX^{EAL} domains (right panel of Fig. 3*a* and Table 3). This strong dependence of complex formation upon c-di-GMP is also observed in gel chromatography on Superdex 75, as shown in Fig. 3(*b*). In the absence of c-di-GMP, gel chromatography of a mixture of *Xcc*FimX^{EAL} and *Xcc*PilZ$_{1028}$ domain proteins gave two major peaks eluting at the expected volumes for monomers (shown in red), with a small proportion of the total protein eluting at the volume expected for a complex. However, in the presence of c-di-GMP (shown in blue) almost all of the protein is eluted as a single peak at an elution volume corresponding to a molecular weight of 94.5 kDa. The calculated molecular weight is only 10% less than the expected molecular weight of the (*Xcc*PilZ$_{1028}$)$_2$–(*Xcc*FimX^{EAL}–c-di-GMP)$_2$ heterotetramer complex as observed in the crystal structure. Given the highly symmetrical peak shape and the absence of higher mass oligomerized material, we assume that the *Xcc*PilZ$_{1028}$–*Xcc*FimX^{EAL}–c-di-GMP complex is a heterotetramer. The results of these two different experiments clearly demonstrate that the type II *Xcc*PilZ$_{1028}$ domain binds to the *Xcc*FimX^{EAL} domain in a 1:1 ratio when c-di-GMP is present but shows little binding in the absence of the nucleotide.

3.4. A type II *Xcc*PilZ$_{1028}$ domain induces dimerization of the *Xcc*FimX^{EAL} domain *via* helix swapping to form an (*Xcc*PilZ$_{1028}$)$_2$–(*Xcc*FimX^{EAL}–c-di-GMP)$_2$ heterotetrameric complex

As described above, c-di-GMP is found to be an important mediator in uniting the *Xcc*FimX^{EAL} and *Xcc*PilZ$_{1028}$ domains. The reasons why c-di-GMP is indispensable became clear when the crystal structure of the *Xcc*PilZ$_{1028}$–c-di-GMP–*Xcc*FimX^{EAL} ternary complex was solved (Fig. 4*a*), which revealed an (*Xcc*PilZ$_{1028}$)$_2$–(*Xcc*FimX^{EAL}–c-di-GMP)$_2$ heterotetrameric complex structure. The two *Xcc*PilZ$_{1028}$ domains (shown in magenta and red, respectively) interact with the two *Xcc*FimX^{EAL} domains (shown in marine and cyan, respectively) mainly through residues Val68 and Thr70 in the β4 strand of the *Xcc*PilZ$_{1028}$ domain and residues Ser53 and Met51 in the β2′ strand of the *Xcc*FimX^{EAL} domain to form a pseudo-continuous β1–β2–β2′–β4–β5–β2 β-sheet (circled in red in Fig. 4*a* and expanded in Fig. 4*b*). Other interactions between the *Xcc*PilZ$_{1028}$ β5 strand and the *Xcc*FimX^{EAL} α3 helix are also observed. Another important aspect in forming such a stable ternary complex is the domain swapping of the N-terminal *Xcc*FimX^{EAL} α1 helices induced by binding of the *Xcc*PilZ$_{1028}$ domain. This domain swapping, which is circled in orange in Fig. 4(*a*) and expanded in Fig. 4(*c*), significantly increases the buried surface between the two *Xcc*FimX^{EAL} domains to approximately 1500 Å, with a Δ^iG value of 78.2 kJ mol^{-1} as calculated using the program *PISA* (Krissinel & Henrick, 2007). This is significant as the *Xcc*FimX^{EAL} domain tends to form a monomer in the absence of the *Xcc*PilZ$_{1028}$ domain (Fig. 3). The domain swapping starts at the hinge residue Gly20 at the beginning of the β1 strand (annotated in red in Fig. 4*c*) and turns either leftwards (marked by a red dotted arrow) in the *Xcc*FimX^{EAL}–c-di-GMP complex (grey cartoons) to form a more compact β-barrel structure in the absence of the *Xcc*PilZ$_{1028}$ domain or turns rightwards (marked by a blue dotted arrow) to interact with the α2 and α3 helices of the opposite *Xcc*FimX^{EAL} subunit (marine cartoons) in the *Xcc*PilZ$_{1028}$–c-di-GMP–*Xcc*FimX^{EAL} ternary complex (Fig. 4*d*). We note with interest that the backbones of the *Xcc*FimX^{EAL} domains in the presence (cyan cartoon in Fig. 4*a*) or absence (grey cartoon) of the *Xcc*PilZ domain superimpose very well after residue Gly20 (the r.m.s.d. between the two domains is only 0.78 Å from Gly20 to Met247). The N-terminal helix α1 of the *Xcc*FimX^{EAL} domain in the *Xcc*PilZ$_{1028}$–c-di-GMP–*Xcc*FimFimX^{EAL} ternary complex is approximately six residues shorter than that in the *Xcc*FimX^{EAL}–c-di-GMP complex after domain swapping because the highly hydrophilic N-terminal ERIERW sequence becomes disordered and is not visible in the map (Fig. 1*a*). However, substantial hydrophobic interactions of residues from the swapped α1 helix (including residues Val9, Leu12, Ala15 and Leu16) with residues from the α2/α3 helices (Ile60, Leu66 and Ile70) and β1/β2 strands (Phe21 and Leu45) of the neighbouring *Xcc*FimX^{EAL} domain are observed (Fig. 4*d*).

3.5. C-di-GMP in the *Xcc*PilZ$_{1028}$–*Xcc*FimX^{EAL}–c-di-GMP ternary complex exhibits a conformation different from that in the *Xcc*FimX^{EAL}–c-di-GMP binary complex

We note with great interest that c-di-GMP is indeed quite flexible and has adopted a different conformation in the *Xcc*PilZ$_{1028}$–*Xcc*FimX^{EAL}–c-di-GMP ternary complex (C atoms in c-di-GMP coloured green) compared with that in the *Xcc*FimX^{EAL}–c-di-GMP complex (c-di-GMP coloured light

grey), as shown in the dotted red rectangle in Fig. 5(*a*) and expanded in Fig. 5(*b*). From this figure, it can be seen that charged residues such as Lys30, Lys66, Asp46 and Glu47 (not shown in Fig. 5*b* to prevent clustering) in the *Xcc*PilZ$_{1028}$

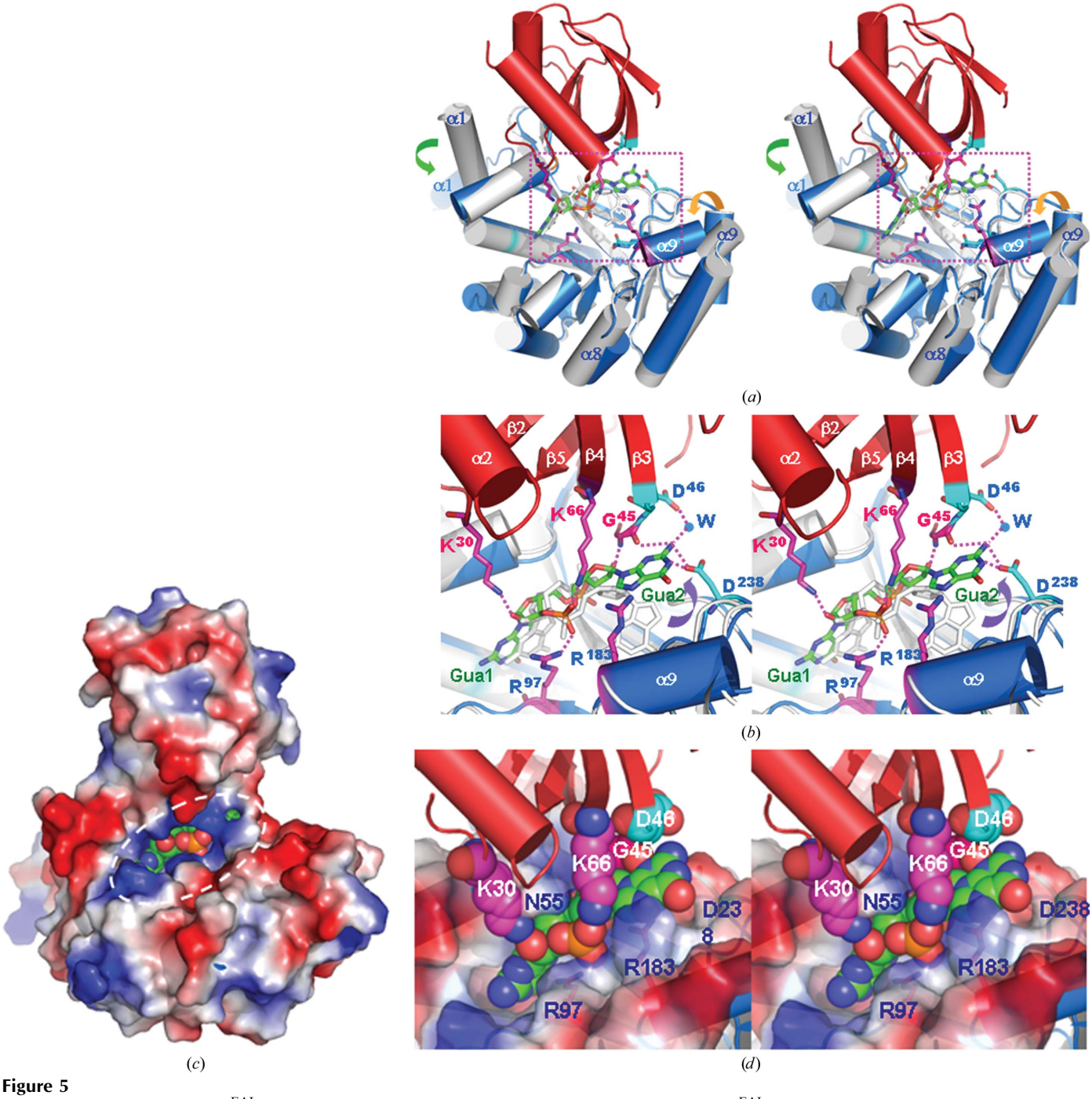

Figure 5
(*a*) Stereoview of the *Xcc*FimX^{EAL}–c-di-GMP–*Xcc*PilZ$_{1028}$ complex superimposed with the *Xcc*FimX^{EAL}–c-di-GMP complex. *Xcc*PilZ$_{1028}$ is shown in cartoon representation in red, *Xcc*FimX^{EAL} in blue and the C atoms of c-di-GMP in green in the ternary complex, while *Xcc*FimX^{EAL} is shown in cartoon representation in grey and the C atoms of c-di-GMP are shown in grey in the binary complex. The major interaction region between the *Xcc*FimX^{EAL}–c-di-GMP complex and *Xcc*PilZ$_{1028}$ is boxed by a dotted magenta square. The α9 helix and α1 helix in the *Xcc*FimX^{EAL} domain exhibit considerable conformational changes after *Xcc*PilZ$_{1028}$ binding and are indicated by orange and green curved arrows, respectively. (*b*) The expanded interface region shown in stereo. A different open-twisted conformation of c-di-GMP in the ternary complex is observed and its C atoms are shown in green, while the open-*syn* c-di-GMP in the binary complex is shown in grey for comparison. Residues Lys30, Lys66, Gly45 and Asp46 from the *Xcc*PilZ$_{1028}$ domain and residues Arg97 and Asp238 from the *Xcc*FimX^{EAL} domain important for c-di-GMP binding are shown in stick representation. (*c*) c-di-GMP (drawn as van der Waals spheres) is found to fit well into the interface between the *Xcc*FimX^{EAL} and *Xcc*PilZ$_{1028}$ domains. It is enclosed by a highly positively charged region, which is circled by a dotted white line and expanded in (*d*). (*d*) Expanded interface view of the *Xcc*FimX^{EAL} domain shown as electrostatic potential; the *Xcc*PilZ$_{1028}$ domain is shown as a cartoon representation in red. Important residues described above for c-di-GMP interaction are shown as van der Waals spheres to reveal the close contact between these interacting residues.

domain are fully extended outwards and may be located within interacting distance of the similarly charged residues Arg97, Arg183 and Asp238 in the *Xcc*FimX^{EAL} domain (see Supplementary Fig. S2). However, when c-di-GMP is present it interacts extensively with the side-chain atoms of residues Lys30 and Lys66 of the *Xcc*PilZ$_{1028}$ domain and the side-chain atoms of residues Arg97 and Asp238 of the *Xcc*FimX^{EAL} domain, which can help in neutralizing the repulsive interactions between the two similarly charged domains. In addition, Gua2 of c-di-GMP is now exposed and interacts well with the backbone atoms of Gly45 and the side-chain atoms of Asp46 (*via* a bound water molecule marked by a blue circle in Fig. 5*b*) of the *Xcc*PilZ$_{1028}$ domain and with the side-chain atoms of Asp238 of the *Xcc*FimX^{EAL} domain. Thus, the now fully extended open c-di-GMP molecule acts as an insulator to neutralize the repulsive force between the *Xcc*PilZ$_{1028}$ and *Xcc*FimX^{EAL} domains. This scenario can account for the strong binding of the *Xcc*PilZ$_{1028}$ domain to *Xcc*FimX^{EAL} in the presence of c-di-GMP. The interactions between the *Xcc*FimX^{EAL}–*Xcc*PilZ$_{1028}$ complex and c-di-GMP are shown in Supplementary Table S2 and as a *LigPlot* representation in Supplementary Fig. S5.

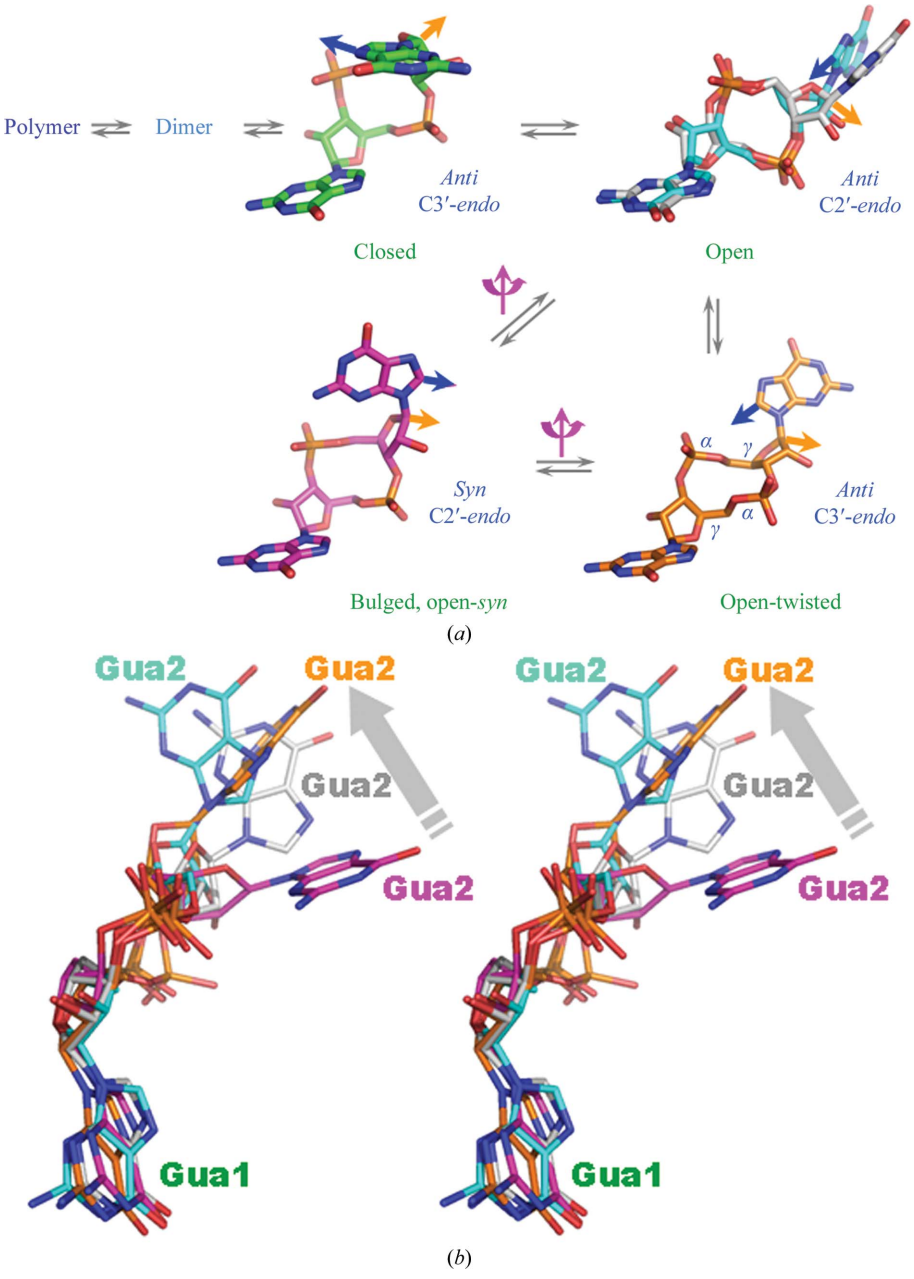

Figure 6
Structural polymorphism of c-di-GMP. (*a*) C-di-GMP can adopt different polymerization states or a monomeric state in equilibrium, but only a monomer or dimer is detected under physiological conditions in a microbial cell. The dimer can adopt a mutually intercalated or partially intercalated form arising from the closed monomer form (Yang *et al.*, 2011), which can be converted to other open monomer forms. The open-*syn* form and the open-twisted forms observed in this study can be transformed by a 180° glycosidic bond rotation (indicated by a curved magenta arrow) and by the interconversion of the sugar pucker from C2′-*endo* to C3′-*endo*. The ribose H1′ proton and the Gua2 base H8 proton are indicated by orange and blue arrows, respectively. (*b*) Superimposition of different monomeric c-di-GMP conformations in stereo. Considerable differences in the Gua2 base orientation are evident from this figure when the Gua1 bases are superimposed. C atoms of c-di-GMP are coloured magenta for the *Xcc*FimX^{EAL}–c-di-GMP binary complex, orange for the *Xcc*FimX^{EAL}–c-di-GMP–*Xcc*PilZ$_{1028}$ ternary complex, grey for the *Pa*FimX^{EAL}–c-di-GMP binary complex and cyan for the *Pf*LapD^{EAL}–c-di-GMP binary complex.

Amazingly, no major conformational change is observed for the *Xcc*PilZ$_{1028}$ domain, except that the extended charged residues such as Lys30, Lys66 and Glu47 have adopted different rotamer conformations in order to better interact with the embedded c-di-GMP (marked by curved red arrows in Supplementary Fig. S2). Similarly, only a few residues of the *Xcc*FimX^{EAL} domain such as Asp71, Lys97, Glu159, Lys183, Phe217 and Asp238 adopt different rotamer conformations to better interact with the embedded c-di-GMP even when the glycosidic bond of Gua2 adopts a different *anti* conformation after *Xcc*PilZ$_{1028}$ binding. The importance of Lys30, Lys66 and Gly45 in the *Xcc*PilZ$_{1028}$ domain are clearly revealed by ITC and gel-filtration chromatography experiments with substitution mutants (Supplementary Fig. S3). When these residues were altered to alanine, the *Xcc*PilZ$_{1028}$ domain lost its ability to bind to the *Xcc*FimX^{EAL}–c-di-GMP complex (Supplementary Fig. S3*a*) and the *Xcc*PilZ$_{1028}$ variants and the *Xcc*FimX^{EAL}–c-di-GMP component eluted from the column at their monomeric volumes in a gel-filtration experiment

(Supplementary Fig. S3*b*). While ITC cannot be relied upon to give accurate values of weak affinities, it is sensitive enough to distinguish a significant loss of affinity upon mutation.

4. Discussion

4.1. Structural polymorphism of c-di-GMP

The novel c-di-GMP conformation observed in the *Xcc*FimX^{EAL}–c-di-GMP complex structure is different from that of the closed form (in which the two guanine bases are on the same face; Fig. 6*a*) commonly found when the nucleotide binds to a type I PilZ domain (Benach *et al.*, 2007; Habazettl *et al.*, 2011) or that of the fully extended and open conformation (in which the two guanine bases are on different faces; Fig. 6*b*) identified to date in binding to active or degenerate EAL domains (Benach *et al.*, 2007; Navarro *et al.*, 2009; Ko *et al.*, 2010; Habazettl *et al.*, 2011). Fig. 6(*a*) shows that the bulged or open-*syn* form and the open-twisted form of c-di-GMP can be interconverted by a 180° flip of the Gua2 base around the glycosidic bond and by transformation of the sugar pucker from C2′-*endo* to C3′-*endo*. Such a *syn*-cyclic nucleotide conformation is not unprecedented and has been observed in the second adenine base located close to DNA in the structure of a CAP–DNA complex containing two c-AMP molecules bound to each monomer (Passner & Steitz, 1997). In order to further examine the conformational differences among these open-form c-di-GMPs, we superimposed their Gua1 bases to observe the differences in the position of the second Gua2 base. As shown in Fig. 6(*b*) (the C atoms of c-di-GMP in the *Pa*FimX^{EAL} and *Pf*LapD^{EAL} domains are drawn in grey and cyan, respectively), the orientations of Gua2 in the *Xcc*-FimX^{EAL}–c-di-GMP and the *Xcc*PilZ$_{1028}$–*Xcc*FimX^{EAL}–c-di-GMP complexes are flipped by approximately 90° around, and are oriented almost perpendicularly to the Gua2 bases of the other two open c-di-GMP conformations (PDB entries 3pjt and 3hv8; Fig. 2*c*; Navarro *et al.*, 2009, 2011). Thus, four unique monomeric c-di-GMP conformations have been observed to date: a closed form when bound to the canonical type I PilZ domain (Benach *et al.*, 2007; Habazettl *et al.*, 2011), an open form when bound to active (Minasov *et al.*, 2009; Tchigvintsev *et al.*, 2010) or degenerate (Navarro *et al.*, 2009, 2011) EAL domains, and the open-*syn* and open-twisted forms present in the *Xcc*FimX^{EAL}–c-di-GMP and *Xcc*PilZ$_{1028}$–*Xcc*FimX^{EAL}–c-di-GMP complexes reported in the present manuscript.

4.2. Comparison of the c-di-GMP binding sites of the *Xcc*FimX^{EAL}, *Pa*FimX^{EAL} and *Pf*LapD^{EAL} domains

In order to understand why the c-di-GMP binding mode of *Xcc*FimX^{EAL} differs from those of the degenerate *Pa*FimX^{EAL} and *Pf*LapD^{EAL} domains, we compared their binding patterns in detail as shown in Supplementary Fig. S1, in which the different stacking patterns of the Gua2 base with the E^{216}FVA^{219} motif, the P^{651}FVE^{654} motif and the E^{617}RVE^{620} motif in the *Xcc*FimX^{EAL}, *Pa*FimX^{EAL} and *Pf*LapD^{EAL} domains, respectively, as well as the different binding patterns to the phosphate moieties are clearly shown. From this comparison, one can understand why Gua2 of c-di-GMP adopts a buried and bulged state in the *Xcc*FimX^{EAL} domain but prefers an exposed state in the *Pa*FimX^{EAL} and *Pf*LapD^{EAL} domains. Gua2 of c-di-GMP in the *Pa*FimX^{EAL} or *Pf*LapD^{EAL} domains is stacked with a polar residue such as Tyr673 or Gln639 on the surface, which allows Gua2 to be lifted up towards the protein surface (Supplementary Figs. S1*b* and S1*c*). However, Gua2 of c-di-GMP in the *Xcc*FimX^{EAL} domain is stacked with the hydrophobic residue Phe217, which partially accounts for the buried conformation of Gua2 in the *Xcc*FimX^{EAL}–c-di-GMP complex. Moreover, it is the first residue Glu216 in the E^{216}FVA motif of *Xcc*FimX^{EAL} that forms two hydrogen bonds to the buried Gua2 (Supplementary Fig. S1*a*). However, in the *Pa*FimX^{EAL} or *Pf*LapD^{EAL} domain it is the last residue Glu654 or Glu620 in the PFVE^{654} or ERVE^{620} motif that interacts with Gua2 (Supplementary Figs. S1*b* and S1*c*). The different positions of the glutamate residue in these crucial tetraresidue motifs seems to play an important role in promoting different c-di-GMP conformations in the several FimX^{EAL}–c-di-GMP complex structures determined to date (see Supplementary Table S2).

4.3. Two different PilZ domains control the flagellum-dependent or pilus-dependent motility

We note with interest that the two PilZ domains involved in flagellum-dependent or pilus-dependent motility are of different types. The PilZ domain that directly interacts with c-di-GMP and affects the flagellar-driven motility is of type I and its N-terminal end undergoes considerable conformational changes upon c-di-GMP binding. This can be revealed by comparison of the apo and c-di-GMP-bound forms of PA4608, which is a type I PilZ protein with conserved R*xxx*R and D*x*D*xx*G signature motifs at the N-terminal end (Habazettl *et al.*, 2011). Upon c-di-GMP binding, its N-terminal residues (1–14) undergo a 90° flip at the hinge Ile14 residue (shown by a blue curved arrow in Supplementary Fig. S6*a*) in order for the signature motif residues Arg8 and Arg10 to bind to c-di-GMP. Another example is VCA0042, which is another type I PilZ protein containing two YcgR domains with a conserved c-di-GMP signature motif linking the two domains. In its apo-form state, the N-terminal PilZ domain is almost detached from the C-terminal YcgR domain (see Fig. 4 of Benach *et al.*, 2007). However, after c-di-GMP binding the two domains are found in close association, with the c-di-GMP molecule tightly packed in their mutual interface. This seems to be a general phenomenon that occurs when c-di-GMP binds to a type I PilZ domain. In contrast, the PilZ domain interacting with FimX and PilB is of type II, lacking the c-di-GMP binding signature motif, and only binds to c-di-GMP indirectly when assisted by the FimX^{EAL} domain. The type II PilZ domain also does not undergo significant backbone conformational change when bound to the FimX^{EAL}–c-di-GMP complex (see Supplementary Figs. S2 and S6*b*). Only some side chains such as those of Lys30, Lys66 and Glu47 adopt different rotamer conformations to interact with c-di-GMP (Supplementary Fig. S2). Similarly, the backbone of the

*Xcc*FimX^{EAL} domain interacting with c-di-GMP also does not exhibit large conformational changes (Supplementary Fig. S2). In contrast, it is the c-di-GMP that changes its conformation to fit into the binding interface and to form the stable *Xcc*PilZ$_{1028}$–*Xcc*FimX–c-di-GMP ternary complex. It remains to be seen whether $K^{30}X_nK^{66}$ (where *X* represents any amino acid) and $G^{45}D^{46}E^{47}$ of *Xcc*PilZ$_{1028}$ form the characteristic interacting signature motifs of type II PilZ-domain sequences (Supplementary Fig. S2).

5. Conclusion

In conclusion, the present manuscript discusses several interesting issues. Firstly, the crystal structure of the *Xcc*FimFimX^{EAL}–c-di-GMP complex contains a novel bulged or open-*syn* c-di-GMP conformation, while that of the *Xcc*FimFimX^{EAL}–c-di-GMP–*Xcc*PilZ$_{1028}$ complex exhibits another open-twisted c-di-GMP conformation. Along with the reported open and closed forms, this structural polymorphism of c-di-GMP indicates that the energy barrier between these different c-di-GMP monomeric conformations is not significant and the distinct form that it takes depends on the effector molecules that it encounters. The flexibility of c-di-GMP thus plays an important role in its interaction with the various downstream effectors. Secondly, unlike the type I PilZ domain, which can bind c-di-GMP strongly and undergo significant conformational change, the type II *Xcc*PilZ$_{1028}$ domain does not bind c-di-GMP or purified *Xcc*FimX^{EAL} domain well, but binds the *Xcc*FimX^{EAL}–c-di-GMP complex strongly without a major global conformational change of the *Xcc*FimX^{EAL} domain and the type II PilZ domain itself. Thirdly, the type II *Xcc*PilZ$_{1028}$ domain induces a different *Xcc*FimX^{EAL} dimerization mode by swapping the *Xcc*-FimX^{EAL} α1 helix and changing the position of its α9 helix for better c-di-GMP binding (Fig. 5*a*). How the *Xcc*FimX^{EAL}–c-di-GMP–*Xcc*PilZ$_{1028}$ complex binds PilB ATPase and acts to control T4P biogenesis and motility remains unclear and deserves further investigation.

This work was supported in part by the Ministry of Education, Taiwan, ROC under the ATU plan and by the National Science Council, Taiwan, ROC (grants 97-2113-M005-005-MY3) to SHC. We appreciate the service of the Structural Genomics Databases provided by the GMBD Bioinformatics Core (http://www.tbi.org.tw), NRPGM, Taiwan, ROC. We would also like to thank the Core Facilities for Protein X-ray Crystallography in the Academia Sinica, Taiwan, ROC for help in crystal screening and the National Synchrotron Radiation Research Center (NSRRC) in Taiwan and the SPring-8 Synchrotron facility in Japan for assistance with the X-ray data collections. The National Synchrotron Radiation Research Center is a user facility supported by the National Science Council, Taiwan, ROC and the Protein Crystallography Facility is supported by the National Research Program for Genomic Medicine, Taiwan, ROC. We would also like to thank Dr Zhao-Xun Liang and Ms Mary Lay-Cheng Chuah at the University of Singapore for their generous gift of c-di-GMP.

References

Adams, P. D. *et al.* (2010). *Acta Cryst.* D**66**, 213–221.
Alm, R. A., Bodero, A. J., Free, P. D. & Mattick, J. S. (1996). *J. Bacteriol.* **178**, 46–53.
Benach, J., Swaminathan, S. S., Tamayo, R., Handelman, S. K., Folta-Stogniew, E., Ramos, J. E., Forouhar, F., Neely, H., Seetharaman, J., Camilli, A. & Hunt, J. F. (2007). *EMBO J.* **26**, 5153–5166.
Boehm, A., Kaiser, M., Li, H., Spangler, C., Kasper, C. A., Ackermann, M., Kaever, V., Sourjik, V., Roth, V. & Jenal, U. (2010). *Cell*, **141**, 107–116.
Chin, K.-H., Lee, Y.-C., Tu, Z.-L., Chen, C.-H., Tseng, Y.-H., Yang, J.-M., Ryan, R. P., McCarthy, Y., Dow, J. M., Wang, A. H.-J. & Chou, S.-H. (2010). *J. Mol. Biol.* **396**, 646–662.
Fang, X. & Gomelsky, M. (2010). *Mol. Microbiol.* **76**, 1295–1305.
Guzzo, C. R., Salinas, R. K., Andrade, M. O. & Farah, C. S. (2009). *J. Mol. Biol.* **393**, 846–866.
Habazettl, J., Allan, M. G., Jenal, U. & Grzesiek, S. (2011). *J. Biol. Chem.* **286**, 14304–14314.
Hengge, R. (2009). *Nature Rev. Microbiol.* **7**, 263–273.
Huang, B., Whitchurch, C. B. & Mattick, J. S. (2003). *J. Bacteriol.* **185**, 7068–7076.
Jenal, U. & Malone, J. (2006). *Annu. Rev. Genet.* **40**, 385–407.
Kazmierczak, B. I., Lebron, M. B. & Murray, T. S. (2006). *Mol. Microbiol.* **60**, 1026–1043.
Ko, J., Ryu, K.-S., Kim, H., Shin, J.-S., Lee, J.-O., Cheong, C. & Choi, B.-S. (2010). *J. Mol. Biol.* **398**, 97–110.
Krissinel, E. & Henrick, K. (2007). *J. Mol. Biol.* **372**, 774–797.
La Fortelle, E. de & Bricogne, G. (1997). *Methods Enzymol.* **276**, 472–494.
Li, T.-N., Chin, K.-H., Fung, K.-M., Yang, M.-T., Wang, A. H.-J. & Chou, S.-H. (2011). *PLoS One*, **6**, e22036.
Li, T.-N., Chin, K.-H., Liu, J.-H., Wang, A. H.-J. & Chou, S.-H. (2009). *Proteins*, **75**, 282–288.
Li, T.-N., Chin, K.-H., Shih, H.-L., Wang, A. H.-J. & Chou, S.-H. (2009). *Acta Cryst.* F**65**, 1056–1059.
Liao, Y.-T., Chin, K.-H., Kuo, W.-T., Chuah, M. L.-C., Liang, Z.-X. & Chou, S.-H. (2012). *Acta Cryst.* F**68**, 301–305.
Mattick, J. S. (2002). *Annu. Rev. Microbiol.* **56**, 289–314.
McCarthy, Y., Ryan, R. P., O'Donovan, K., He, Y.-Q., Jiang, B.-L., Feng, J.-X., Tang, J.-L. & Dow, J. M. (2008). *Mol. Plant Pathol.* **9**, 819–824.
McRee, D. E. (1999). *J. Struct. Biol.* **125**, 156–165.
Minasov, G., Padavattan, S., Shuvalova, L., Brunzelle, J. S., Miller, D. J., Baslé, A., Massa, C., Collart, F. R., Schirmer, T. & Anderson, W. F. (2009). *J. Biol. Chem.* **284**, 13174–13184.
Murshudov, G. N., Skubák, P., Lebedev, A. A., Pannu, N. S., Steiner, R. A., Nicholls, R. A., Winn, M. D., Long, F. & Vagin, A. A. (2011). *Acta Cryst.* D**67**, 355–367.
Navarro, M. V., De, N., Bae, N., Wang, Q. & Sondermann, H. (2009). *Structure*, **17**, 1104–1116.
Navarro, M. V., Newell, P. D., Krasteva, P. V., Chatterjee, D., Madden, D. R., O'Toole, G. A. & Sondermann, H. (2011). *PLoS Biol.* **9**, e1000588.
Otwinowski, Z. & Minor, W. (1997). *Methods Enzymol.* **276**, 307–326.
Passner, J. M. & Steitz, T. A. (1997). *Proc. Natl Acad. Sci. USA*, **94**, 2843–2847.
Paul, K., Nieto, V., Carlquist, W. C., Blair, D. F. & Harshey, R. M. (2010). *Mol. Cell*, **38**, 128–139.
Qi, Y., Chuah, M. L. C., Dong, X., Xie, K., Luo, Z., Tang, K. & Liang, Z.-X. (2011). *J. Biol. Chem.* **286**, 2910–2917.
Rao, F., Pasunooti, S., Ng, Y., Zhuo, W., Lim, L., Liu, A. W. & Liang, Z.-X. (2009). *Anal. Biochem.* **389**, 138–142.
Römling, U. (2011). *Environ. Microbiol.* **14**, 1817–1829.
Römling, U. & Amikam, D. (2006). *Curr. Opin. Microbiol.* **9**, 218–228.

Römling, U., Gomelsky, M. & Galperin, M. Y. (2005). *Mol. Microbiol.* **57**, 629–639.
Ryan, R. P., Tolker-Nielsen, T. & Dow, J. M. (2012). *Trends Microbiol.* **20**, 235–242.
Schirmer, T. & Jenal, U. (2009). *Nature Rev. Microbiol.* **7**, 724–735.
Smith, K. D., Shanahan, C. A., Moore, E. L., Simon, A. C. & Strobel, S. A. (2011). *Proc. Natl Acad. Sci. USA*, **108**, 7757–7762.
Sondermann, H., Shikuma, N. J. & Yildiz, F. H. (2011). *Curr. Opin. Microbiol.* **15**, 140–146.
Sterner, R. & Höcker, B. (2005). *Chem. Rev.* **105**, 4038–4055.
Tchigvintsev, A., Xu, X., Singer, A., Chang, C., Brown, G., Proudfoot, M., Cui, H., Flick, R., Anderson, W. F., Joachimiak, A., Galperin, M. Y., Savchenko, A. & Yakunin, A. F. (2010). *J. Mol. Biol.* **402**, 524–538.
Thormann, K. M. & Paulick, A. (2010). *Microbiology*, **156**, 1275–1283.
Tuckerman, J. R., Gonzalez, G. & Gilles-Gonzalez, M.-A. (2011). *J. Mol. Biol.* **407**, 622–639.
Wang, J., Zhou, J., Donaldson, G. P., Nakayama, S., Yan, L., Lam, Y., Lee, W. T. & Sintim, H. O. (2010). *J. Am. Chem. Soc.* **133**, 9320–9330.
Wu, Y.-Y., Chin, K.-H., Chou, C.-C., Lee, C.-C., Shr, H.-L., Gao, F. P., Lyu, P.-C., Wang, A. H.-J. & Chou, S.-H. (2005). *Acta Cryst.* F**61**, 902–905.
Yang, C.-Y., Chin, K.-H., Chuah, M. L.-C., Liang, Z.-X., Wang, A. H.-J. & Chou, S.-H. (2011). *Acta Cryst.* D**67**, 997–1008.
Zhang, Z., Kim, S., Gaffney, B. L. & Jones, R. A. (2006). *J. Am. Chem. Soc.* **128**, 7015–7024.